Ziyou Song
State Key Laboratory of Automotive Safety and Energy, Tsinghua University, Beijing 100084, China; Department of Electrical Engineering and Computer Science, University of Michigan, Ann Arbor, MI 48109
e-mail: ziyou.songthu@gmail.com

Heath Hofmann
Department of Electrical Engineering and Computer Science, University of Michigan, Ann Arbor, MI 48109

Jianqiu Li
State Key Laboratory of Automotive Safety and Energy, Tsinghua University, Beijing 100084, China; Collaborative Innovation Center of Electric Vehicles in Beijing, Beijing 100081, China

Yuanying Wang
Department of Electrical Engineering and Computer Science, University of Michigan, Ann Arbor, MI 48109

Dongbin Lu
NR Electric Co., Ltd., Nanjing 211102, China

Minggao Ouyang
State Key Laboratory of Automotive Safety and Energy, Tsinghua University, Beijing 100084, China

Jiuyu Du[1]
State Key Laboratory of Automotive Safety and Energy, Tsinghua University, Beijing 100084, China
e-mail: dujiuyu@tsinghua.edu.cn

Torque Distribution Strategy for Multi-PMSM Applications and Optimal Acceleration Control for Four-Wheel-Drive Electric Vehicles

In this paper, a general torque distribution strategy is proposed to improve the drivetrain efficiency of four-wheel-drive electric vehicles (EVs). The strategy allows the same or different motors to be equipped in the front and rear wheels. The model of the drivetrain considers the loss properties of four permanent magnet synchronous motors (PMSMs) and four inverters over a wide range of torque and speed. The relationship between the drivetrain efficiency and the torque split ratio at any given speed is proven to be convex under both traction and regenerative braking conditions. It is shown that, when all four motors are identical, the maximum efficiency can be achieved if the total torque is equally shared. An equivalent loss strategy, which is a general method and can solve many optimization problems of multi-PMSM applications, is proposed to maximize the drivetrain efficiency when different PMSMs are used in the front and rear wheels. The effectiveness of the proposed strategy is verified using an urban dynamometer driving schedule (UDDS). In addition, the acceleration process of EVs is optimized using a dynamic programming approach to minimize acceleration duration and energy consumption. Simulation results show that, with the proposed strategy, the energy loss during the acceleration can be reduced by up to 15%. [DOI: 10.1115/1.4045321]

Keywords: four-wheel-drive, electric vehicle, torque split strategy, optimal acceleration control, dynamic programming, multi-PMSM applications

1 Introduction

Given present consumption rates, it has been estimated that the current global petroleum resources will be used up within 50 years [1]. Electric vehicles (EVs), which are receiving considerable attention, are effective solutions for energy and environmental problems [2]. The electrified and intelligent transportation system has been extensively studied as the effective solution for the aforementioned problem [3,4]. Other advantages of EVs over internal combustion engine vehicles are [5,6]:

(1) the torque response of electric motors is 10–100 times faster than that of engines,
(2) all wheels can be independently controlled by adopting small- and high-power in-wheel motors, and
(3) the output torque of an electric motor can be estimated from motor currents.

The four-wheel-drive (4WD) EV under study is a microsized two-seat car of ~660-kg curb weight. As shown in Fig. 1 [7], each wheel of this EV is equipped with a permanent-magnet synchronous motor (PMSM) controlled independently by a vehicle control unit (VCU) and a motor control unit (MCU). It has been identified that the PMSM has the highest power density and efficiency when compared with dc and induction motors [8,9]. Motion control is implemented by the VCU, and torque commands are transferred to the MCUs via a controller area network (CAN) bus [10].

With respect to longitudinal motion, the four-wheel-drive EV provides one degree-of-freedom in torque distribution (between front and rear wheels) for improving the drivetrain efficiency. This issue is important because EV mileage is still limited by

[1]Corresponding author.

Contributed by the Dynamic Systems Division of ASME for publication in the Journal of Dynamic Systems, Measurement, and Control. Manuscript received February 28, 2018; final manuscript received October 18, 2019; published online November 14, 2019. Assoc. Editor: Junmin Wang.

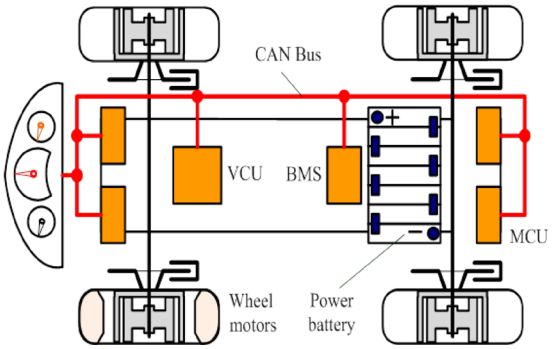

Fig. 1 Configuration of the four-wheel-drive EV [7]

battery capacity [11–13]. The modeling and design of the drivetrain for a single-motor drive EV has been illustrated in Ref. [14], and motor loss minimization is presented in Ref. [15]. Compared with the single-motor configuration, a multimotor configuration realizes more flexible dynamic control [16] and achieves a better dynamic performance, such as acceleration stability [17], braking stability [18], and lateral stability [19]. Novellis et al. proposed the optimal wheel torque distribution for a 4WD EV to minimize tire slip [20]. In addition, the multimotor configuration provides redundancy to improve reliability and fail-safe operation [21].

Furthermore, the multimotor configuration enables power sharing between different motors, which has the potential to increase EV efficiency. Based on the energy loss model of a permanent-magnet (PM) motor, the torque distribution scheme of the front- and rear-wheel-driven EV, where two PM motors are coupled to the front and rear axles, is investigated in Ref. [21]. The relationship between motor efficiency and its torque at a given speed is derived and shows that, when four identical motors are used, the maximum efficiency can be achieved if the total torque is equally shared [21]. Wang et al. developed a prototype four-wheel-drive EV and proposed a numerical solution to improve the EV efficiency by appropriately allocating the total required torque among the four in-wheel motors [22]. Wu et al. used dynamic programming (DP) approach to deal with the torque split problem of a dual-motor powertrain and found that the energy consumption rate of the proposed method can be reduced by around 6% [23]. Bao et al. focused on the regenerative braking condition and compared different operation modes (i.e., front motor only, rear motor only, and both motors) to increase system efficiency and vehicle stability [24]. Hu et al. optimized the motor sizes of a dual-motor powertrain and compared the optimal design with common designs [25]. Wu et al. compared the efficiency of the single motor system and the dual motor system [26]. Lin and Xu constructed a multi-objective optimization framework to improve vehicle maneuverability and reduce energy consumption simultaneously [27]. Dizqah et al. formulated the optimal torque distribution as the solution of a parametric optimization problem, based on the vehicle speed [28]. Park et al. developed the fuzzy logic control algorithm to optimize driving efficiency, satisfy driver demands, and consider tire slip [29]. Wang et al. proposed an optimal torque distribution algorithm for longitudinal motion, considering the weight transfer between front and rear axles and motor losses [30]. Guo et al. presented a torque distribution algorithm aiming to reduce energy consumption and improve road handling as well as ride comfortability [31]. Yang et al. adopted particle swarm theory for minimizing energy consumption according to the motor efficiency maps [32].

However, the losses of the motor inverters are not well considered in the above papers. Furthermore, the general torque distribution strategy related to the multimotor configuration where front and rear motors are different is absent in the previous studies. In the general case, different motors may be equipped in front and rear wheels to achieve a more flexible dynamic performance. Small motors can save more space for the steering system of the EV when they are equipped on the front wheels. Furthermore, when the motors equipped on the front wheels are small, an active front steering system is much more flexible because the inertia of the wheel is reduced [33]. Thus, the four-wheel-drive EV equipped with different-sized motors may be promising in autonomous vehicle applications.

To further improve EV efficiency, the total torque curve during EV acceleration should also be carefully designed to minimize acceleration duration and energy consumption [34]. The conflicting nature of reducing energy consumption and acceleration duration is verified in Ref. [35]. It is shown that adopting multiple accelerations during speed changes can reduce energy consumption more than applying a constant acceleration value [36]. However, it is difficult for the driver to accurately track the velocity curve during acceleration. An optimal driving strategy for EVs during speed changes is proposed through multi-objective optimization of various conflicting objectives (acceleration duration, energy consumption, and total jerk) [37]. However, complex computations cannot be avoided to obtain the Pareto-optimal fronts (the computation time was found to be around 1 s [37]); thus, it is still hard to implement this algorithm in real-time applications.

In this paper, a torque distribution strategy is proposed for the four-wheel-drive EV based on the energy loss models of the PMSM and inverter. The relationship between the drivetrain efficiency and the torque split ratio at any given speed is derived and proven to be convex. The optimal torque split ratio is derived by solving the mathematical problem based on energy loss models. It is shown that the maximum efficiency is achieved if the total required torque is equally shared between four identical motors. The equivalent loss rate strategy (ELRS) is proposed in this paper to maximize the drivetrain efficiency when different PMSMs are used. The average-split strategy (ASS), corresponding to the case where all motors are the same, is a special case of the ELRS. The effectiveness of the proposed strategy is verified using a modified urban dynamometer driving schedule (UDDS). In addition, the acceleration process of EVs is optimized using the DP approach to simultaneously minimize acceleration duration and energy consumption. Based on simulation results, some qualitative conclusions are drawn to provide instructional information regarding the EV acceleration control algorithm. When compared to the existing literature, the novelties of this paper can be summarized in three aspects: (1) the inverter energy loss is considered; (2) the analytical solution of the optimal torque split ratio for the case where different PMSMs are used is provided; and (3) the optimal acceleration control algorithm for the 4WD EV is proposed.

This paper is organized as follows: In Sec. 2, the vehicle, PMSM, and energy loss models of the inverters are presented. Section 3 presents a detailed description of the proposed torque distribution strategy and the optimal acceleration strategy. The effectiveness of the proposed algorithms is validated in Sec. 4. Conclusions are presented in Sec. 5.

2 Modeling

2.1 Electric Vehicle Model. Only the longitudinal dynamics are considered in this study, therefore, the dynamics of the four-wheel-drive EV when driving on a flat road can be expressed as

$$\begin{cases} \dfrac{T_{\text{out}}}{r_w} = mgf + \dfrac{1}{2}C_{\text{D}}A_{\text{f}}\rho V^2 + m\dfrac{\text{d}V}{\text{d}t} \\ T_{\text{out}} = T_{\text{e}} - T_{\text{f}} \end{cases} \tag{1}$$

where r is the wheel radius; m is the mass of the vehicle; f is the rolling resistance coefficient; C_{D} is the coefficient of aerodynamic drag; A_{f} is the frontal area exposed to flow; V is the vehicle velocity; $\text{d}V/\text{d}t$ is the vehicle acceleration; ρ is the air density; and T_{out}, T_{e}, and T_{f} are the total output, electromagnetic, and frictional torque of the motor, respectively. We point out that this paper mainly

focuses on the power flow of the system rather than the vehicle dynamic performance. Therefore, the tire model, e.g., magic formulation and "relaxation length" formulation) is not considered in the formulation given that the tire dynamics will not significantly influence the EV power demand. In addition, since both the in-wheel motors and traction wheels are small and no reducer is adopted in between, the rotor inertia and the wheel inertia are also neglected in the formulation for simplification.

2.2 Energy Loss Model of the Permanent Magnet Synchronous Motor. The voltage, flux, and electromagnetic torque equations of the basic PMSM model can be illustrated in Eqs. (2)–(4) [7]. We note that the core losses, which are considered in the energy loss model of PMSM in the sequel, are neglected in these equations

$$\begin{cases} u_d = R_a i_d + \dfrac{d\psi_d}{dt} - \omega\psi_q \\ u_q = R_a i_q + \dfrac{d\psi_q}{dt} + \omega\psi_d \end{cases} \tag{2}$$

$$\begin{cases} \psi_d = L_d i_d + \psi_f \\ \psi_q = L_q i_q \end{cases} \tag{3}$$

$$T_e = n_p(\psi_d i_q - \psi_q i_d) = n_p i_q[\psi_f + (L_d - L_q) i_d] \tag{4}$$

where u_d and u_q are the d- and q-axis terminal voltages, respectively, i_d and i_q are the d- and q-axis armature currents, respectively, L_d and L_q are the d- and q-axis inductances, respectively, R_a is the armature resistance, ω is the electrical angular velocity, Ψ_d and Ψ_q are the d- and q-axis flux-linkages, respectively, Ψ_f is the permanent magnet flux-linkage, and n_p is the number of pole-pairs. Without loss of generality, i_d and i_q can be expressed as

$$\begin{cases} i_q = \sqrt{\dfrac{3}{2}} k I_m \\ i_d = -\sqrt{\dfrac{3}{2}}\sqrt{(1-k^2)} I_m \end{cases} \tag{5}$$

where I_m is the peak value of the sinusoidal current, and k is a function of ω and varies from 0 to 1. The surface mount PMSM ($L_d = L_q = L$) is adopted in this paper, so Eq. (4) can be simplified. The torque equation is therefore simplified to

$$T_e = A I_m \tag{6}$$

where

$$A = \sqrt{\frac{3}{2}} n_p k \psi_f \tag{7}$$

The energy loss model of the PMSM has been intensively studied [38]. As shown in Eq. (8), the energy loss model consists of three parts: copper loss P_{Cu}, iron loss P_{Fe}, and mechanical loss P_m

$$P_{in} = P_{out} + P_{Cu} + P_{Fe} + P_m \tag{8}$$

where P_{in} and P_{out} are the input and output power of the PMSM, respectively. Steady-state losses P_{Cu}, P_{Fe}, and P_m, which are expressed in the following equations, are functions of T_e and ω:

$$P_{Cu} = R_a\left[\left(i_q + \frac{\omega L_d i_d}{R_i} + \frac{\omega\psi_f}{R_i}\right)^2 + \left(i_d - \frac{\omega L_q i_q}{R_i}\right)^2\right] \tag{9}$$

$$P_{Fe} = \frac{\omega^2}{R_i}\left[(L_d i_d + \psi_f)^2 + (L_q i_q)^2\right] \tag{10}$$

$$P_m = T_f \frac{\omega}{n_p} \tag{11}$$

where R_i is the equivalent iron loss resistance of the PMSM.

2.3 Energy Loss Model of the Inverter. The MOSFET transistor is favorable for low-power EV applications [39]; thus, it is employed in this study. The inverter loss consists of switching loss and conduction loss. High-side and low-side MOSFETs conduct complementarily to control the PMSM. A dead time is inserted between turn-off and turn-on to avoid inverter shoot-through [40]. It is assumed that the MOSFET resistive voltage drop is lower than the body diode voltage drop; hence, when on, it can be assumed that all current flows through the MOSFET resistance.

(1) Conduction loss. The simplified models of the MOSFET and the diode are given in Refs. [7] and [41], as shown in the following equation:

$$\begin{aligned} U_{ds} &= I_{dev} R_{ds} \\ U_{ak} &= U_f + I_{dev} R_{ak} \end{aligned} \tag{12}$$

where U_{ds} and U_{ak} are the on-state voltage drops of the MOSFET and the diode, respectively; U_f is the diode voltage drop at the zero-current condition; R_{ds} and R_{ak} are the resistance of the MOSFET and the diode, respectively; and I_{dev} is the device current. Considering the dead-time effect, the time-averaged conduction loss in the three-phase inverter can be simplified as [36]

$$\begin{cases} P_{c-\text{MOSFETs}} = \dfrac{3}{2} I_m^2 R_{ds}\left(1 - \dfrac{2t_d}{t_c}\right) \\ P_{c-Ds} = \left(\dfrac{6}{\pi} U_f I_m + \dfrac{3}{2} I_m^2 R_{ak}\right)\dfrac{2t_d}{t_c} \end{cases} \tag{13}$$

where t_d is the dead time and t_c is the period of the pulse width modulation. Hence, the conduction loss of the inverter is

$$P_c = P_{c-\text{MOSFETs}} + P_{c-Ds} \tag{14}$$

(2) Switching loss. As shown in Eq. (13), the switching loss of a hard-switched circuit includes two parts [42]

$$\begin{cases} P_{sw-on} = k_{on} I_m f_s/\pi \\ P_{sw-off} = k_{off} I_m f_s/\pi \end{cases} \tag{15}$$

where $P_{sw\text{-}on}$ and $P_{sw\text{-}off}$ are the turn on and the turn off losses, respectively, f_s is the switching frequency, and k_{on} and k_{off} can be determined from the device datasheet and bus voltage. Based on the above analysis, the switching loss of the three-phase inverter can be derived

$$P_{sw} = 3(P_{sw-on} + P_{sw-off}) \tag{16}$$

The total loss of the three-phase inverter, which is the sum of the conduction loss and the switching loss, can then be expressed as

$$\begin{aligned} P_{inv} = &\left[\frac{12 t_d U_f}{\pi t_c} + \frac{3 k_{on} f_s}{\pi} + \frac{3 k_{off} f_s}{\pi}\right] I_m \\ &+ \left[\frac{3 R_{ak} t_d}{t_c} + \frac{3}{2} R_{ds}\left(1 - \frac{2t_d}{t_c}\right)\right] I_m^2 \end{aligned} \tag{17}$$

This shows that the inverter loss P_{inv} is also a function of T_e and ω. By integrating Eq. (5) into Eqs. (9) and (10), we get

$$P_{Cu} = \frac{3}{2}R_a\left[(1-k^2)\left(1+\frac{\omega^2 L_d^2}{R_i^2}\right)+k^2\left(1+\frac{\omega^2 L_q^2}{R_i^2}\right)\right]I_m^2 + \sqrt{6}\frac{R_a\omega\psi_f}{R_i}\left(k-\frac{\omega L_d}{R_i}\sqrt{1-k^2}\right)I_m + R_a\left(\frac{\omega\psi_f}{R_i}\right)^2 \quad (18)$$

$$P_{Fe} = \frac{3}{2}\frac{\omega^2}{R_i}\left[(1-k^2)L_d^2+k^2L_q^2\right]I_m^2 - \sqrt{6}\frac{\omega^2}{R_i}\sqrt{1-k^2}\psi_f L_d I_m + \frac{\omega^2\psi_f^2}{R_i} \quad (19)$$

Based on Eqs. (10)–(12) and (18)–(19), the PMSM and inverter losses can be simplified to

$$\begin{aligned} P_{Cu}+P_{Fe}+P_m &= BI_m^2+CI_m+D \\ P_{inv} &= XI_m^2+YI_m \end{aligned} \quad (20)$$

where

$$\begin{aligned} B &= \frac{3}{2}R_a\left[(1-k^2)\left(1+\frac{\omega^2L_d^2}{R_i^2}\right)+k^2\left(1+\frac{\omega^2L_q^2}{R_i^2}\right)\right] + \frac{3}{2}\frac{\omega^2}{R_i}\left[(1-k^2)L_d^2+k^2L_q^2\right] \\ C &= \sqrt{6}\frac{R_a\omega\psi_f}{R_i}\left(k-\frac{\omega L_d}{R_i}\sqrt{1-k^2}\right)-\sqrt{6}\frac{\omega^2}{R_i}\sqrt{1-k^2}\psi_f L_d \\ D &= (R_a+R_i)\left(\frac{\omega\psi_f}{R_i}\right)^2+\frac{T_f\omega}{n_p} \\ X &= \left[\frac{3R_{ak}t_d}{t_c}+\frac{3}{2}R_{ds}\left(1-\frac{2t_d}{t_c}\right)\right] \\ Y &= \left[\frac{12t_dU_f}{\pi t_c}+\frac{3k_{on}f_s}{\pi}+\frac{3k_{off}f_s}{\pi}\right] \end{aligned} \quad (21)$$

Based on Eq. (20), the loss power for one motor and its inverter can be given as

$$P_{Cu}+P_{Fe}+P_m+P_{inv} = (B+X)I_m^2+(C+Y)I_m+D \quad (22)$$

Thus, the second derivative of the motor loss with respect to T_e can be derived as

$$\frac{\partial^2(P_{Cu}+P_{Fe}+P_m+P_{inv})}{\partial T_e^2} = 2(B+X)\left(\frac{\partial I_m}{\partial T_e}\right)^2 + 2(B+X)I_m\frac{\partial^2 I_m}{\partial T_e^2}+(C+Y)\frac{\partial^2 I_m}{\partial T_e^2} \quad (23)$$

Based on Eq. (6), we see that

$$\begin{aligned} \frac{\partial I_m}{\partial T_e} &= \frac{1}{A} \\ \frac{\partial^2 I_m}{\partial T_e^2} &= 0 \end{aligned} \quad (24)$$

By integrating Eq. (24) into Eq. (23), the second derivative of the motor loss with respect to T_e can be derived

$$\frac{\partial^2(P_{Cu}+P_{Fe}+P_m+P_{inv})}{\partial T_e^2} = \frac{2(B+X)}{A^2} \quad (25)$$

Therefore, $\partial^2(P_{Cu}+P_{Fe}+P_m+P_{inv})/\partial T_e^2 > 0$ is satisfied because A, B, and X are always positive, which means that the motor loss with respect to T_e is convex. This conclusion is important to the torque split strategy presented in Sec. 3.

3 Optimal Torque Distribution and Acceleration Control Strategies

3.1 The Torque Distribution Strategy. In this paper, only longitudinal motion of the four-wheel-drive EV is considered, so the torque is assumed to be equally shared between the right and left motors. At each instant, the torque required by the EV is known. We assume that the total required torque is $2T_{dem}$ and define the torque split ratio β as

$$\begin{aligned} T_{ef} &= T_{dem}\beta \\ T_{er} &= T_{dem}(1-\beta) \end{aligned} \quad (26)$$

where T_{ef} and T_{er} are the electromagnetic torque of the front and rear motors, respectively. To find the optimal β for loss minimization, the relationship between β and the total loss power of the drivetrain at a given speed should be derived. As mentioned above, the total loss P_{loss} includes the PMSM loss and the inverter loss. Based on Eqs. (6) and (20), P_{loss} can be simplified to

$$P_{loss} = P_{loss,f}(T_{ef})+P_{loss,r}(T_{er}) \quad (27)$$

where $P_{loss,f}$ and $P_{loss,r}$ are the loss power of the front and rear motors, respectively. The second derivative of P_{loss} with respect to β can be derived as

$$\frac{\partial^2 P_{loss}}{\partial\beta^2} = \frac{\partial^2 P_{loss,f}}{\partial T_{ef}^2}\left(\frac{\partial T_{ef}}{\partial\beta}\right)^2+\frac{\partial P_{loss,f}}{\partial T_{ef}}\frac{\partial^2 T_{ef}}{\partial\beta^2}+\frac{\partial^2 P_{loss,r}}{\partial T_{er}^2}\left(\frac{\partial T_{er}}{\partial\beta}\right)^2 + \frac{\partial P_{loss,r}}{\partial T_{er}}\frac{\partial^2 T_{er}}{\partial\beta^2} \quad (28)$$

Based on Eq. (26), Eq. (28) can be simplified to

$$\frac{\partial^2 P_{loss}}{\partial\beta^2} = \frac{\partial^2 P_{loss,f}}{\partial T_{ef}^2}T_{dem}^2+\frac{\partial^2 P_{loss,r}}{\partial T_{er}^2}T_{dem}^2 \quad (29)$$

As a result, $\partial^2 P_{loss}/\partial\beta^2$ is always positive because both $\partial^2 P_{loss,f}/\partial T_{ef}^2$ and $\partial^2 P_{loss,r}/\partial T_{er}^2$ are positive, which means that the function of P_{loss} with respect to β is convex. Thus, at any given speed and torque, there is an optimal β for minimizing the total loss of the EV drivetrain, and the optimal β occurs when $\partial P_{loss}/\partial\beta$ is zero

$$\frac{\partial P_{loss,f}}{\partial T_{ef}}T_{dem}-\frac{\partial P_{loss,r}}{\partial T_{er}}T_{dem} = 0 \quad (30)$$

The optimal β is therefore obtained when

$$\frac{\partial P_{loss,f}}{\partial T_{ef}} = \frac{\partial P_{loss,r}}{\partial T_{er}} \quad (31)$$

We first consider the case where the motors equipped on the front and rear wheels are identical. Given that $\partial^2 P_{loss,f}/\partial T_{ef}^2$ and $\partial^2 P_{loss,r}/\partial T_{er}^2$ are positive, the following equation can be obtained from Eq. (31):

$$T_{ef} = T_{er} \quad (32)$$

As shown in Eq. (32), the total loss of the EV drivetrain is at a minimum when the front and rear motors equally share the torque under the assumption that all motors are identical, regardless of the values of total torque and EV speed. Note that the basic convex optimization theorem is used to obtain the optimal torque split ratio, as shown in Eq. (31), since the energy loss function is

continuous and the second derivative in terms of the demand torque exists.

In the general case, the front and rear motors may be different; thus, the optimal torque split ratio will change according to the motor parameters. When the front and rear motors are different, the total loss of all motors is at a minimum when the front and rear motors have the same loss rate with respect to their electromagnetic torque, as shown in Eq. (31). The front and rear motors should therefore share the torque according to the ELRS. The ELRS shown in Eq. (31) is still effective in regenerative braking modes because the convex characteristic of the power loss function with respect to β is preserved. We point out that the ELRS proposed in this paper can also be used to solve the optimization problems under the conditions that (1) identical motors work at different speeds, which also cause difference in coefficients shown in Eq. (31), or (2) different motors work at the same or different speeds. There are two approaches to implement the proposed ELRS: (1) calculate the numerical solution based on Eqs. (22) and (31) if all parameters of different motors and the corresponding inverters are well known, and (2) search the optimal solution based on two maps corresponding to different motors, which can be obtained via calibration experiments, and provide the values of $\partial P_{\text{loss,f}}/\partial T_{\text{ef}}$ and $\partial P_{\text{loss,r}}/\partial T_{\text{er}}$. In the following simulation, the first method is adopted to implement the ELRS based on the assumption that all the motors' parameters are well known. To be specific, based on Eq. (22), the power losses of the front and rear motors can be given as

$$\begin{cases} P_{\text{loss,f}} = (B_{\text{f}} + X_{\text{f}})I_{\text{m,f}}^2 + (C_{\text{f}} + Y_{\text{f}})I_{\text{m,f}} + D_{\text{f}} \\ P_{\text{loss,r}} = (B_{\text{r}} + X_{\text{r}})I_{\text{m,r}}^2 + (C_{\text{r}} + Y_{\text{r}})I_{\text{m,r}} + D_{\text{r}} \end{cases} \tag{33}$$

and based on Eqs. (6) and (24), β can be determined given that $\partial P_{\text{loss,f}}/\partial T_{\text{ef}} = \partial P_{\text{loss,r}}/\partial T_{\text{er}}$

$$\beta = \frac{\dfrac{2(B_{\text{r}} + X_{\text{r}})}{A_{\text{r}}^2} + \left[\dfrac{(C_{\text{r}} + Y_{\text{r}})}{A_{\text{r}}} - \dfrac{(C_{\text{f}} + Y_{\text{f}})}{A_{\text{f}}}\right]}{2\left[\dfrac{(B_{\text{f}} + X_{\text{f}})}{A_{\text{f}}^2} + \dfrac{(B_{\text{r}} + X_{\text{r}})}{A_{\text{r}}^2}\right]} \tag{34}$$

We would like to point out that the objectives of torque split strategy and traction control strategy may be contradictory. Specifically, assuming the adoption of the same PMSMs, the torque should be equally split to increase the system efficiency based on the above analysis. However, the traction control system may require another torque split ratio, which is not 0.5 and depends on the vehicle weight distribution and tire-road interfaces, to accelerate the vehicle by fully exploiting the transmissible force.

3.2 Optimal Acceleration Control. To further improve EV performance, the total torque curve should be optimized to reduce energy loss during acceleration. Therefore, it is important to find the optimal acceleration values so that the EV uses the stored battery energy in the most efficient way while performing a speed change. In conventional EVs, a constant PMSM power (CPP) (or a constant PMSM torque), corresponding to the pedal position, is maintained by the VCU and MCU. A DP approach is adopted in this paper to understand the benefits that global optimization can bring to the EV acceleration process [43]. Furthermore, the DP results may provide guidance which can help us to accelerate the EV efficiently in the shortest duration possible.

The EV velocity V is the primary state in the DP process, and V is therefore discretized to 400 states in its operating range (from 0 km/h to 80 km/h), as shown in Fig. 2. In the DP process, the EV is accelerated from its initial speed V_0 to its final speed V_{f} over a time duration t_{acc}. The energy loss of the EV over the acceleration process is calculated and minimized according to the cost function

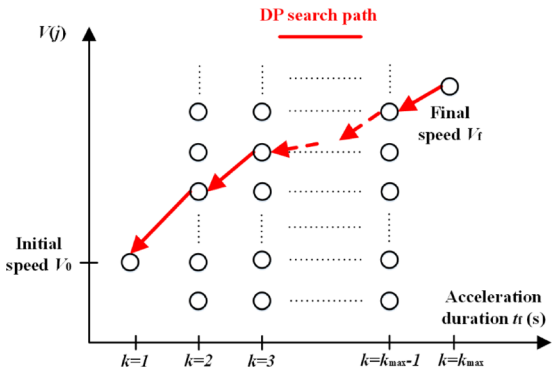

Fig. 2 DP optimization flowchart

Table 1 Basic parameters of the studied four-wheel-drive EV

Parameter	Value
m, EV weight (kg)	660
r, Wheel radius (m)	0.25
f, Rolling coefficient	0.014
C_{D}, Dimensionless coefficient	0.4
A, Frontal area (m^2)	1.4
ρ, Air density (kg/m^3)	1.29

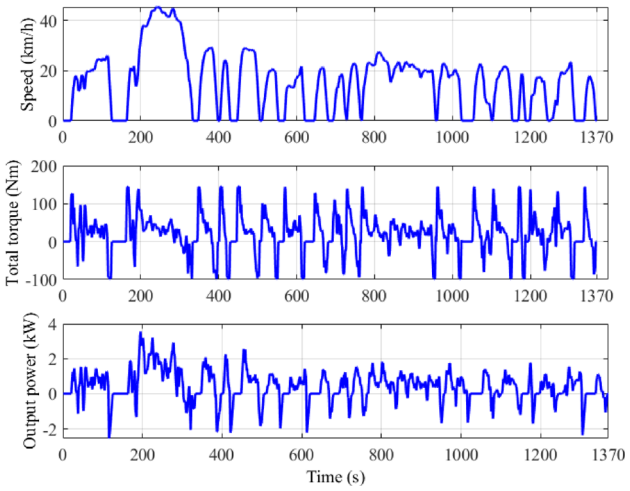

Fig. 3 The speed, torque, and power profiles of the EV along the half UDDS

$$\text{Minimize} \quad \left\{\sum_{k=1}^{k=k_{\max}} P_{\text{loss}}(k)T_{\text{s}}\right\} \tag{35}$$

where T_{s} is the sample time and is set to 1 s in this study, and $P_{\text{loss}}(k)$ is the total loss power of the EV drivetrain from instant k to $k+1$, which is derived from Eq. (20). In order to calculate P_{loss} for each discrete time k, the EV acceleration $a(k)$ is determined as

$$a(k) = \frac{V(k+1) - V(k)}{T_{\text{s}}} \tag{36}$$

By integrating Eq. (36) to Eqs. (1) and (20), P_{loss} can be derived at each instant. Consequently, the minimum energy loss over the acceleration duration can be found by proceeding backward, as shown in Fig. 2.

Table 2 Basic parameters of the three-phase inverter

Parameter	Value
U_f, Diode voltage drop (V)	1.3
R_{ds}, MOSFET resistance (Ω)	5.6×10^{-3}
R_{ak}, Diode resistance (Ω)	1×10^{-4}
t_d, Dead time (s)	3×10^{-6}
f_s, Switching frequency (Hz)	1.6×10^{4}
k_{on}, Switch-on coefficient	5.48×10^{-5}
k_{off}, Switch-off coefficient	1.62×10^{-5}

Table 3 Basic parameters of two PMSMs adopted in this study

Parameter	PMSM #1	PMSM #2
n_p, Pole pairs	23	23
R_a, Armature resistance (Ω)	0.031	0.02
R_i, Iron consumption resistance (Ω)	$1.5 + 0.006\omega$	$1.5 + 0.006\omega$
L_d, d-axis inductance (mH)	0.076	0.076
L_q, q-axis inductance (mH)	0.076	0.076
Ψ_f, Permanent magnet flux-linkage (Wb)	0.0204	0.025
T_f, Friction torque (N·m)	0.2	0.1
T_{max}, Maximum torque (N·m)	80	100
Maximum speed (rpm)	500	500
P_{max}, Maximum power (kW)	2	2.5

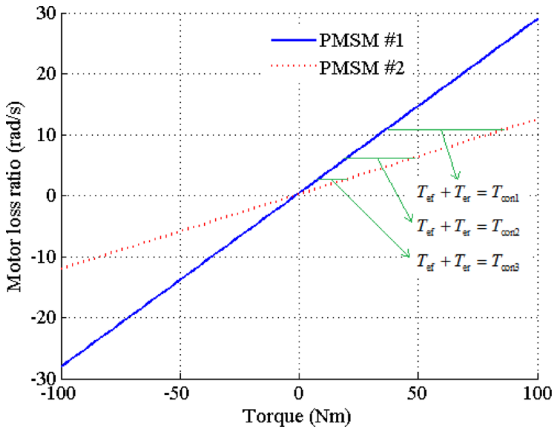

Fig. 5 The motor loss ratio of PMSM #1 and #2 at 250 rpm

4 Simulation Results

4.1 Torque Distribution Strategy. To verify the torque distribution strategy, the energy consumption of an EV should be evaluated over a driving cycle since the drivetrain efficiency varies with torque and speed. The UDDS is adopted in this study; however, the maximum speed of the standard UDDS exceeds that of the EV prototype studied in this paper, which is a low-speed

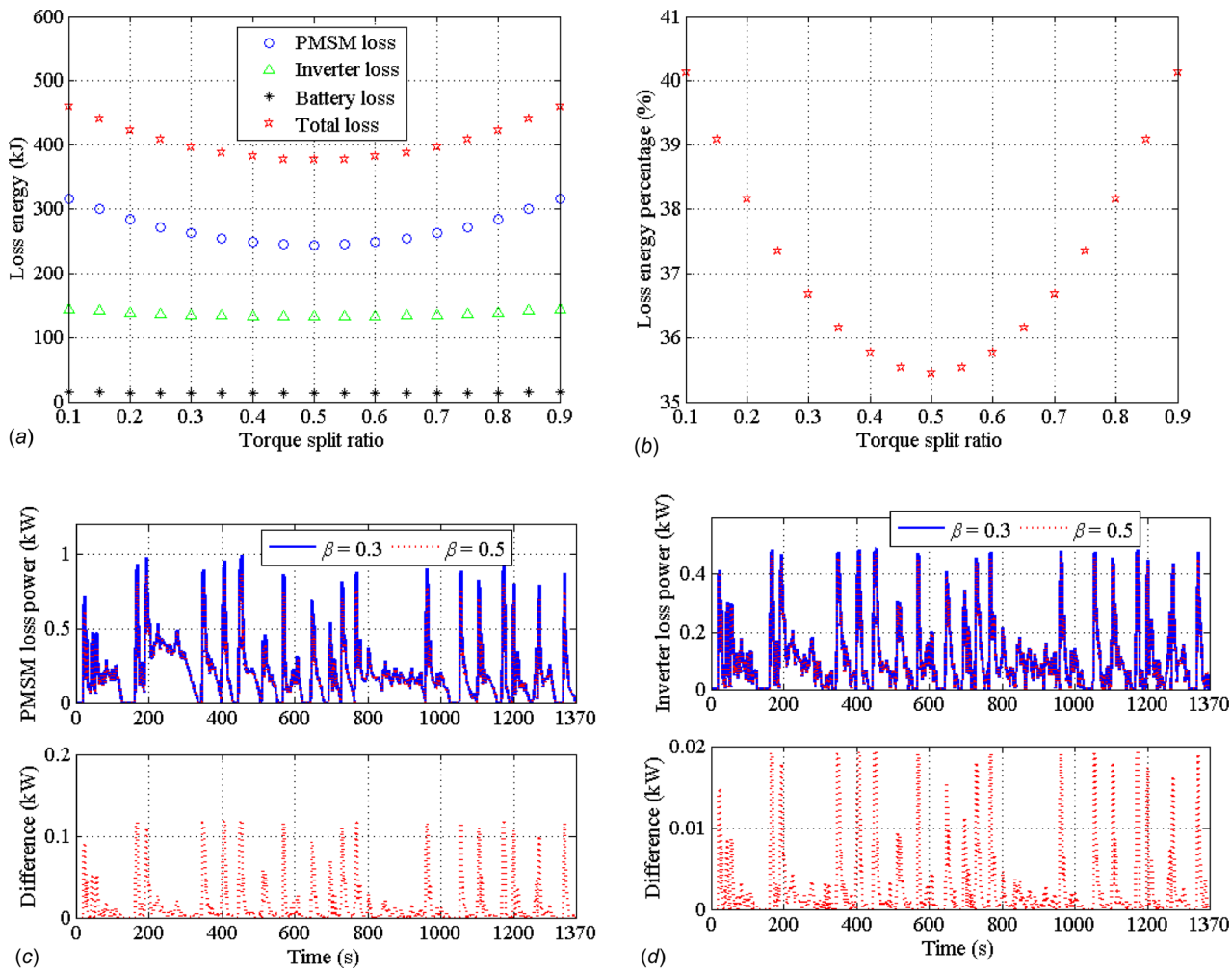

Fig. 4 ASS verification results when all motors are identical: (*a*) loss energy, (*b*) the energy loss percentage of the total energy loss, (*c*) PMSM loss power, and (*d*) inverter loss power

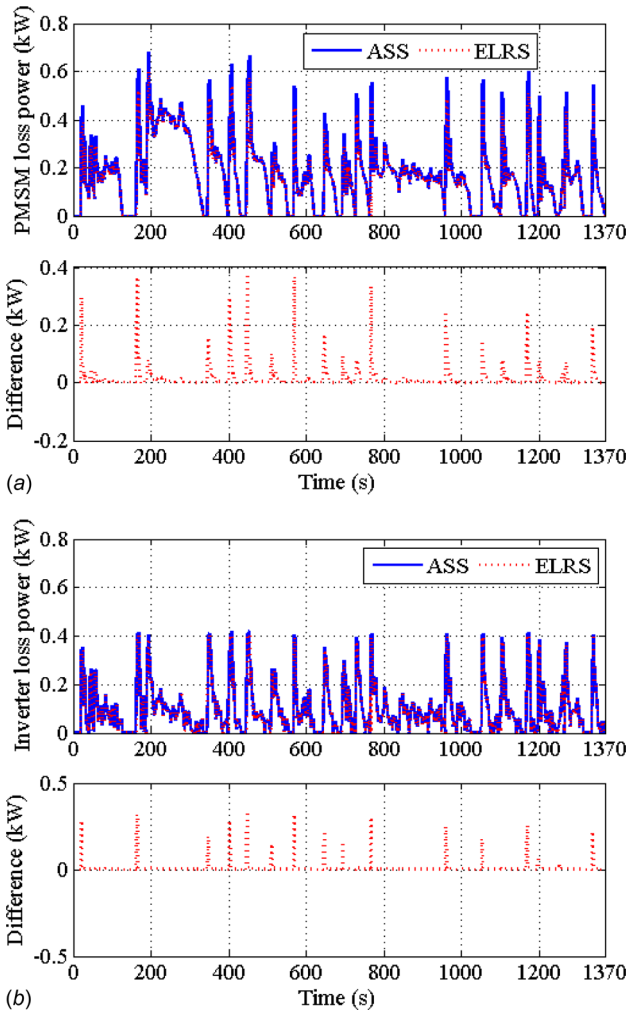

Fig. 6 The comparison result of ASS and ELRS when front and rear motors are different: (*a*) PMSM loss power and (*b*) inverter loss power

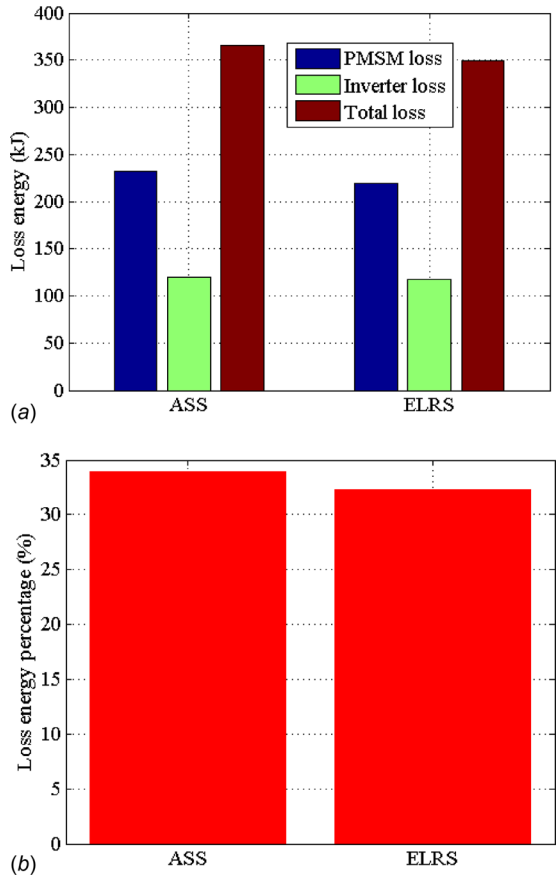

Fig. 7 The energy loss comparison of ASS and ELRS: (*a*) the energy losses from PMSMs and inverters and (*b*) the energy loss percentages of the total energy loss

vehicle. The basic parameters of the four-wheel-drive EV studied in this paper are listed in Table 1.

Therefore, the magnitude of the velocity profile of UDDS is halved in this study. The speed, torque, and power profiles of the EV along the modified drive cycle are shown in Fig. 3. Note that the torque is calculated based on the EV dynamic model, as shown in Eq. (1), and the power can therefore be derived. The regenerative braking efficiency is assumed to be 30% because a mechanical brake is also used [44]. The basic parameters of the inverter used in this study are listed in Table 2.

This study not only examines the torque split strategy when all motors are identical, but also investigates the strategy when the front and rear motors are different. Thus, two different PMSMs are considered in this study, and parameters of PMSM #1 and PMSM #2 are listed in Table 3. Both motors are small (i.e., the maximum power is around 2 kW), as they are used in the micro-sized 4WD EV. Generally, the microsized EV is not designed to have a high dynamic performance, therefore, the EV will not require large torque/power demands from the PMSM. These two PMSMs will be equipped in the front and rear wheels of the studied EV, and the ELRS is used to optimally split the torque to minimize the system energy loss. Note that the motors listed in Table 3 are only employed to establish a case study, and the proposed ELRS can be utilized in any multi-PMSM applications.

The ASS is proven to be optimal when all motors of the EV are identical, based on the analysis in Sec. 3. In the first simulation, all wheels of the EV are equipped with PMSM #1. As shown in Fig. 4(*a*), the total loss energy of the EV drivetrain over the drive cycle, including the losses of PMSM and inverter, achieves the minimum value when the torque split ratio β is 0.5 (ASS). As shown in Fig. 4(*a*), when β varies from 0.3 to 0.7, the variation of the total energy loss is less than 10%. Therefore, the ratios of the energy loss to the total demanded energy are also decreasing when β approaches 0.5, as shown in Fig. 4(*b*). This means that the system efficiency is increased. This difference is mainly caused by the PMSM loss, as shown in Fig. 4(*c*). Compared to the ASS, the PMSM loss power when β is 30% is obviously high in the high-torque regions. And the power loss difference under two split ratios is also indicated in Fig. 4(*c*). In addition, the PMSM loss and the inverter loss account for approximately 63% and 34% of the total loss, which cannot be neglected. The inverter loss is also minimized when the torque split ratio β is 0.5 (ASS), as shown in Fig. 4(*d*). It verifies the convex characteristic of the total inverter loss with respect to β. In the following simulation, the battery energy loss caused by its ohmic resistance is also considered. In this paper, the battery resistance is assumed to be 18 mΩ for the adopted 53 V, 60 Ah Lithium battery pack. The battery loss is less than 5% of the total energy loss and relatively independent of β.

To verify the ELRS shown in Eq. (31), the front and rear wheels are equipped with PMSM #1 and PMSM #2, respectively. As shown in Fig. 5, at a given speed within the normal operating range (flux-weakening region is not considered in the simulation), the PMSM loss rate increases linearly with its electromagnetic torque. At any given torque, different motors have different loss rates. For any required torque, the ELRS can find a set of torque values for front and rear wheels to ensure that they have the same loss rate. For online use, the ELRS can distribute the torque according to the PMSM calibration results.

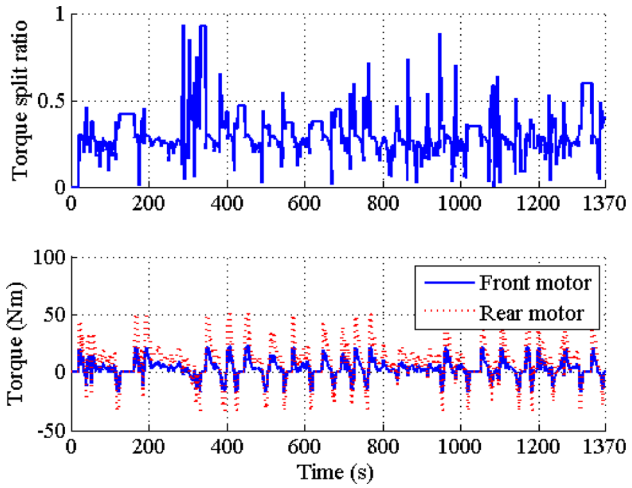

Fig. 8 The torque distribution result of ELRS during the half UDDS

In the simulation, the ELRS is compared with ASS over the drive cycle. As shown in Fig. 6(*a*), the PMSM loss power of the ELRS is lower than that of ASS, especially in high-torque regions. The ELRS and ASS have similar results in terms of inverter loss, as shown in Fig. 6(*b*).

In addition, compared to the ASS, the ELRS reduces the total energy loss over the drive cycle by 4.5%, as shown in Fig. 7(*a*). This means that the system efficiency is increased by using the proposed ELRS, as shown in Fig. 7(*b*). As shown in Fig. 8, the value of torque split ratio β derived from the ELRS is around 0.25. This shows that the optimal torque split ratio can be far from 0.5 when different PMSMs are adopted, and also suggests when ASS is adopted in this application the energy consumption will be significantly increased. Therefore, the torque split ratio should be well considered in multi-PMSM applications. In conclusion, the effectiveness of the proposed torque distribution strategy is validated. The ASS can be adopted when four identical motors are equipped in the EV. Furthermore, the ELRS can be employed to maximize the drivetrain efficiency when different PMSMs are used in the front and rear wheels.

4.2 Optimal Acceleration Control. Acceleration often occurs in EV operation, and the output torque curve should be carefully designed to minimize both energy loss and acceleration duration. The DP presented in Sec. 4 is adopted here to optimize the EV acceleration performance. The CPP strategy, which is commonly used in EVs, is compared with DP in the analysis. The PMSM power of the CPP strategy is directly determined by the position of the acceleration pedal, and this may be a map diagram in the real EVs. The maximum power ability of the studied EV is 8 kW. Note that the proposed torque split strategy is directly adopted in the optimal acceleration control to ensure the optimal distribution of torque.

First, V_0, V_f, and t_{acc} are set to 20 km/h, 57 km/h, and 40 s in the simulation, respectively. The simulation results are shown in Fig. 9, revealing that the speed curves generated by DP and CPP are very different. The CPP yields a concave speed curve, while the DP yields a convex curve. The acceleration duration of DP is slightly less than that of CPP. As shown in Fig. 9(*b*), the total power used in the acceleration process is relatively constant when the EV is controlled by the CPP. In contrast, the total power when the EV is controlled by DP is strictly increasing. This phenomenon can be also seen in Fig. 9(*c*).

In the efficiency map of the PMSM plus the inverter, we can see that the PMSM torque decreases with increasing speed when the CPP is used. In contrast, the DP result shows that the PMSM

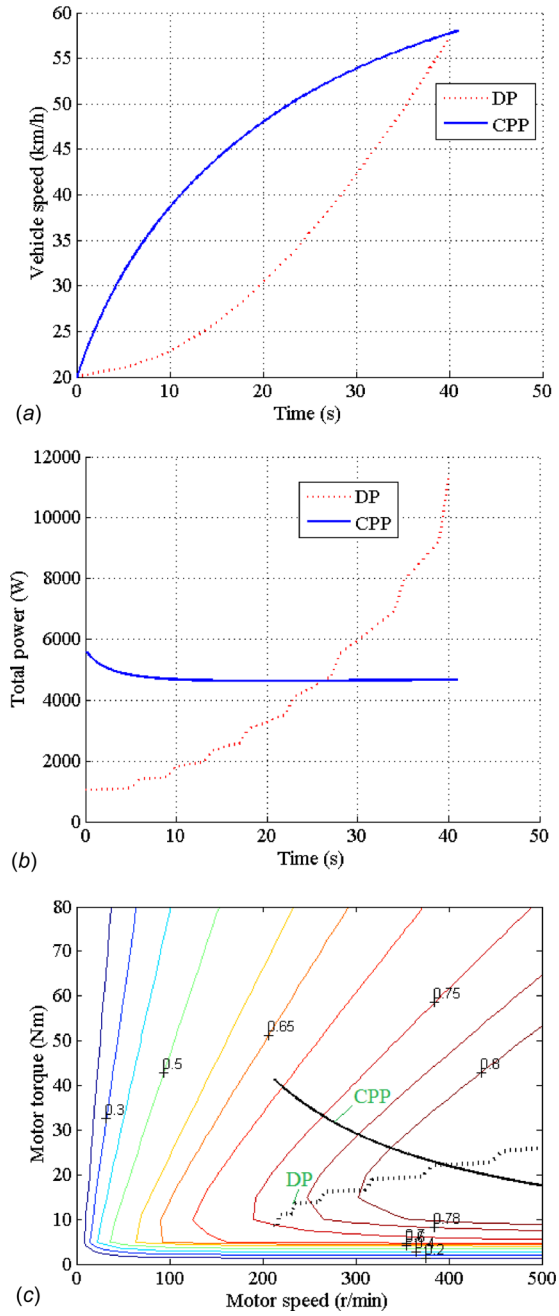

Fig. 9 Simulation results when V_0 is 20 km/h, V_f is 57 km/h, and t_{acc} is 40 s: (*a*) EV speed curves, (*b*) total power curves, and (*c*) motor operation curves

torque slowly increases with increasing speed. It can be seen that high efficiency in the low-torque region is important since much of the energy consumed over the drive cycle is in the low-torque region. Compared with CPP, DP can improve the EV efficiency by utilizing the low-torque region (the incipient stage of the acceleration process), which is highly significant. The total energy loss during the acceleration process is calculated by integrating the energy loss in each interval, based on Eq. (20). The total energy loss corresponding to different acceleration strategies is then compared. Specifically, the total energy losses of CPP and DP during the acceleration process are 37.7 kJ and 35.7 kJ, respectively. Thus, DP decreases the energy loss by 5.3%, while it also reduces the acceleration duration.

In the DP process, t_{acc} can have various values to achieve different acceleration performance. To reduce the acceleration

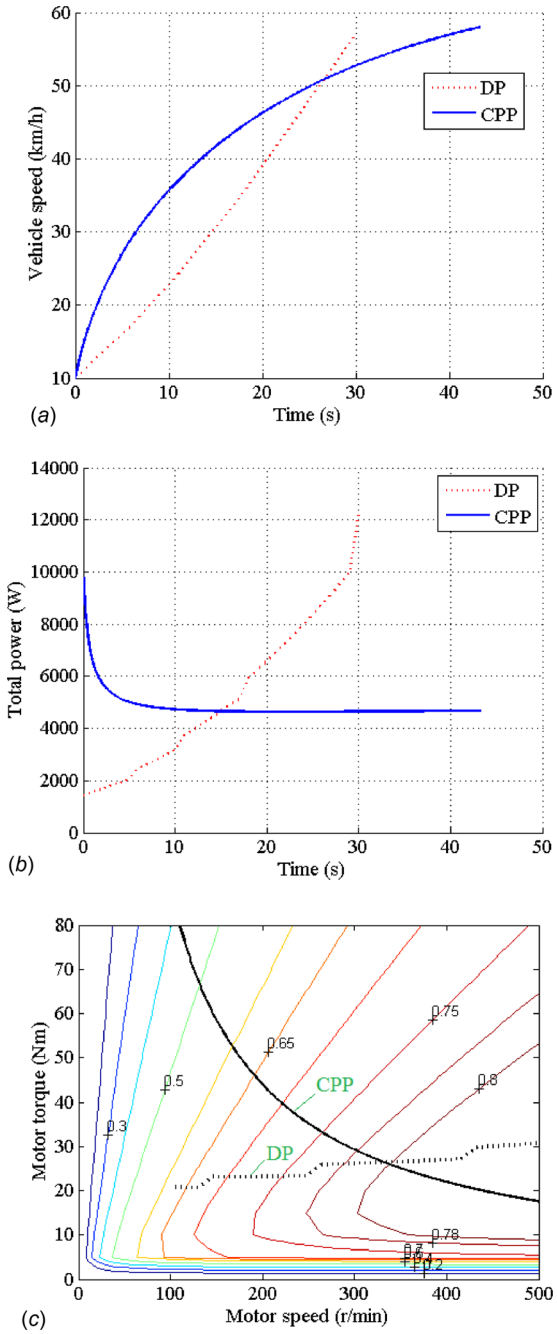

Fig. 10 Simulation results when V_0 is 10 km/h, V_f is 57 km/h, and t_{acc} is 30 s: (*a*) EV speed curves, (*b*) total power curves, and (*c*) motor operation curves

duration, V_0 and t_{acc} are set to 10 km/h and 30 s in the second case, respectively, while the final speed is not changed. The simulation results are shown in Fig. 10. The acceleration duration of DP is much shorter than that of CPP, as shown in Fig. 10(*a*). In comparison with simulation results of the first case, similar results can be found in Figs. 10(*b*) and 10(*c*). The simulation results of the second case also show that DP achieves high efficiency. Moreover, the energy losses of CPP and DP are 44.4 kJ and 37.5 kJ; thus, DP decreases the energy loss by 15.5%. Consequently, the effectiveness of the proposed DP is verified. Even though the energy loss is dominated by the PMSM, we point out that the influence of the inverter energy loss cannot be neglected. Specifically, for the case shown in Fig. 9, the energy losses of inverter for the DP and CPP are 9.23 kJ and 14.66 kJ, respectively, and they account for 26% and 39% of the total energy losses. For the case shown in Fig. 10, the energy losses of the inverter for the DP and CPP are 9.90 kJ and 12.38 kJ, respectively, and they account for 26% and 28% of the total energy loss. Therefore, the inverter loss also significantly influences the system efficiency, especially for the case shown in Fig. 9.

We point out that it is difficult to directly use the proposed algorithm in real application considering the uncertainties in the command velocity profiles, and specific algorithms are required to handle the uncertainty online [45]. However, the DP results can be potentially used to improve the translation of acceleration pedal to torque commands. Specifically, the proposed DP generates a convex curve, indicating the acceleration of the EV is increasing, as shown in Figs. 9(*a*) and 10(*a*). In contrast, the CPP generates a concave curve. However, we point out that the CPP is preferred from the perspective of vehicle dynamics performance as it can control the EV to approach the target speed in a smoother way, while the driver has to brake at the last moment when DP is adopted. To solve this problem, a "jerk" term can be added in the cost function of DP to ensure that the EV speed approaches V_f smoothly. Due to space limitation, this modified DP is not presented in this paper. By directly using simulation results, we may be able to generate a convex-concave speed curve to balance the system efficiency and EV dynamic performance.

5 Conclusion and Future Work

This paper proposes a general torque distribution strategy to improve the drivetrain efficiency of four-wheel-drive EVs regardless of whether the same or different motors are equipped in the front and rear wheels. The PMSM and the inverter models are considered over a wide range of torque and speed. The relationship between drivetrain efficiency and the torque split ratio at any given speed is proven to be convex in the traction mode. It has been shown that the total required torque should be equally shared between four identical motors to maximize the drivetrain efficiency. In addition, the ELRS is proposed for the case when different PMSMs are used. The effectiveness of the proposed strategy is verified over the scaled UDDS. In addition, to save more energy, the EV acceleration process is optimized using DP to minimize both acceleration duration and energy consumption, and the optimal torque split strategy is integrated in the acceleration control. Simulation results show that the proposed strategy can improve the EV efficiency. The energy loss during the acceleration process can be reduced by up to 15%, and the acceleration duration can be significantly reduced. Even though it is difficult to directly adopt the acceleration control strategy in practical applications, simulation results can be used to improve the translation of the position of acceleration pedal.

The contributions of this paper can be summarized in three aspects: (1) the inverter energy loss is considered in the entire model of the 4WD EV powertrain; (2) the analytical solution of the optimal torque split ratio for the case where different PMSMs are used is provided; and (3) the optimal acceleration profile is proposed. When compared with ASS, which has been widely used in four-wheel-drive EVs, the ELRS is a general method, which can be widely used in many multi-PMSM applications, such as hybrid electric vehicle applications. This will be investigated in future work.

Funding Data

- National Science Foundation (Grant No. 51275264; Funder ID: 10.13039/100000001).
- Ministry of Education (Research of Distributed Hybrid Powertrain for Heavy Duty Trucks).

References

[1] Khaligh, A., and Li, Z., 2010, "Battery, Ultracapacitor, Fuel Cell, and Hybrid Energy Storage Systems for Electric, Hybrid Electric, Fuel Cell, and Plug-In Hybrid Electric Vehicles: State of the Art," IEEE Trans. Veh. Technol., **59**(6), pp. 2806–2814.

[2] Jin, L. W., Lee, P. S., Kong, X. X., Fan, Y., and Chou, S. K., 2014, "Ultra-Thin Minichannel LCP for EV Battery Thermal Management," Appl. Energy, **113**, pp. 1786–1794.
[3] Feng, S., Zhang, Y., Li, S. E., Cao, Z., Liu, H. X., and Li, L., 2019, "String Stability for Vehicular Platoon Control: Definitions and Analysis Methods," Annu. Rev. Control, **47**, pp. 81–97.
[4] Feng, S., Wang, X., Sun, H., Zhang, Y., and Li, L., 2018, "A Better Understanding of Long-Range Temporal Dependence of Traffic Flow Time Series," Phys. A: Stat. Mech. Appl., **492**, pp. 639–650.
[5] Maeda, K., Fujimoto, H., and Hori, Y., 2012, "Four-Wheel Driving-Force Distribution Method Based on Driving Stiffness and Slip Ratio Estimation for Electric Vehicle With In-Wheel Motors," IEEE Vehicle Power and Propulsion Conference, , Seoul, South Korea, Oct. 9-12, pp. 1286–1291.
[6] Song, Z., Li, J., Ouyang, M., Gu, J., Feng, X., and Lu, D., 2013, "Rule-Based Fault Diagnosis of Hall Sensors and Fault-Tolerant Control of PMSM," Chin. J. Mech. Eng., **26**(4), pp. 813–822.
[7] Gu, J., Ouyang, M., Lu, D., Li, J., and Lu, L., 2013, "Energy Efficiency Optimization of Electric Vehicle Driven by In-Wheel Motors," Int. J. Automot. Technol., **14**(5), pp. 763–772.
[8] Chau, K. T., Chan, C. C., and Liu, C., 2008, "Overview of Permanent-Magnet Brushless Drives for Electric and Hybrid Electric Vehicles," IEEE Trans. Ind. Electron., **55**(6), pp. 2246–2257.
[9] Chen, J. T., Zhu, Z. Q., Iwasaki, S., and Deodhar, R. P., 2011, "A Novel Hybrid-Excited Switched-Flux Brushless AC Machine for EV/HEV Applications," IEEE Trans. Veh. Technol., **60**(4), pp. 1365–1373.
[10] Li, J., Song, Z., Shuai, Z., Xu, L., and Ouyang, M., 2015, "Wheel Slip Control Using Sliding-Mode Technique and Maximum Transmissible Torque Estimation," ASME J. Dyn. Syst., Meas., Control, **137**(11), p. 111010.
[11] Capasso, C., and Veneri, O., 2014, "Experimental Analysis on the Performance of Lithium Based Batteries for Road Full Electric and Hybrid Vehicles," Appl. Energy, **136**, pp. 921–930.
[12] Rangaraju, S., De Vroey, L., Messagie, M., Mertens, J., and Van Mierlo, J., 2015, "Impacts of Electricity Mix, Charging Profile, and Driving Behavior on the Emissions Performance of Battery Electric Vehicles: A Belgian Case Study," Appl. Energy, **148**, pp. 496–505.
[13] Song, Z., Hofmann, H., Li, J., Hou, J., Zhang, X., and Ouyang, M., 2015, "The Optimization of a Hybrid Energy Storage System at Subzero Temperatures: Energy Management Strategy Design and Battery Heating Requirement Analysis," Appl. Energy, **159**, pp. 576–588.
[14] Morrison, P., Binder, A., Funieru, B., and Sabirin, C., 2009, "Drive Train Design for Medium-Sized Zero Emission Electric Vehicles," 13th European Conference on Power Electronics and Applications, Barcelona, Spain, Sept. 8–10, pp. 1–10.
[15] Mapelli, F. L., Tarsitano, D., and Mauri, M., 2010, "Plug-In Hybrid Electric Vehicle: Modeling, Prototype Realization, and Inverter Losses Reduction Analysis," IEEE Trans. Ind. Electron., **57**(2), pp. 598–607.
[16] Song, Z., Li, J., Wei, Y., Xu, L., and Ouyang, M., 2015, "Interaction of In-Wheel Permanent Magnet Synchronous Motor With Tire Dynamics," Chin. J. Mech. Eng., **28**(3), pp. 470–478.
[17] Osborn, R. P., and Shim, T., 2006, "Independent Control of All-Wheel-Drive Torque Distribution," Veh. Syst. Dyn., **44**(7), pp. 529–546.
[18] Mutoh, N., 2012, "Driving and Braking Torque Distribution Methods for Front- and Rear-Wheel-Independent Drive-Type Electric Vehicles on Roads With Low Friction Coefficient," IEEE Trans. Ind. Electron., **59**(10), pp. 3919–3933.
[19] Zhai, L., Sun, T., and Wang, J., 2016, "Electronic Stability Control Based on Motor Driving and Braking Torque Distribution for a Four In-Wheel Motor Drive Electric Vehicle," IEEE Trans. Veh. Technol., **65**(6), pp. 4726–4739.
[20] De Novellis, L., Sorniotti, A., and Gruber, P., 2013, "Optimal Wheel Torque Distribution for a Four-Wheel-Drive Fully Electric Vehicle," SAE Int. J. Passenger Cars-Mech. Syst., **6**(1), pp. 128–136.
[21] Yuan, X., Wang, J., and Colombage, K., 2012, "Torque Distribution Strategy for a Front and Rear Wheel Driven Electric Vehicle," Sixth IET International Conference on Power Electronics, Machines and Drives, Bristol, UK, Mar. 27–29.
[22] Wang, R., Chen, Y., Feng, D., Huang, X., and Wang, J., 2011, "Development and Performance Characterization of an Electric Ground Vehicle With Independently Actuated In-Wheel Motors," J. Power Sources, **196**(8), pp. 3962–3971.
[23] Wu, X., Zheng, D., Wang, T., and Du, J., 2019, "Torque Optimal Allocation Strategy of All-Wheel Drive Electric Vehicle Based on Difference of Efficiency Characteristics Between Axis Motors," Energies, **12**(6), p. 1122.
[24] Bao, R., Griggs, P., and Baxter, J., 2018, "Simulation Based Control Strategy Design of All Wheel Drive Electric Vehicle Regenerative Braking System," SAE Paper No. 2018-01-0411.
[25] Hu, X., Li, Y., Lv, C., and Liu, Y., 2019, "Optimal Energy Management and Sizing of a Dual Motor-Driven Electric Powertrain," IEEE Trans. Power Electron., **34**(8), pp. 7489–7501.
[26] Wu, J., Liang, J., Ruan, J., Zhang, N., and Walker, P. D., 2018, "Efficiency Comparison of Electric Vehicles Powertrains With Dual Motor and Single Motor Input," Mech. Mach. Theory, **128**, pp. 569–585.
[27] Lin, C., and Xu, Z., 2015, "Wheel Torque Distribution of Four-Wheel-Drive Electric Vehicles Based on Multi-Objective Optimization," Energies, **8**(5), pp. 3815–3831.
[28] Dizqah, A. M., Lenzo, B., Sorniotti, A., Gruber, P., Fallah, S., and De Smet, J., 2016, "A Fast and Parametric Torque Distribution Strategy for Four-Wheel-Drive Energy-Efficient Electric Vehicles," IEEE Trans. Ind. Electron., **63**(7), pp. 4367–4376.
[29] Park, J., Jang, I., and Hwang, S. H., 2018, "Torque Distribution Algorithm for an Independently Driven Electric Vehicle Using a Fuzzy Control Method: Driving Stability and Efficiency," Energies, **11**(12), p. 3479.
[30] Wang, Y., Fujimoto, H., and Hara, S., 2015, "Torque Distribution-Based Range Extension Control System for Longitudinal Motion of Electric Vehicles by LTI Modeling with Generalized Frequency Variable," IEEE/ASME Trans. Mechatronics, 21(1), 2015.2444651, pp. 443–452.
[31] Guo, L., Lin, X., Ge, P., Qiao, Y., Xu, L., and Li, J., 2017, "Torque Distribution for Electric Vehicle With Four In-Wheel Motors by Considering Energy Optimization and Dynamics Performance," IEEE Intelligent Vehicles Symposium (IV), Los Angeles, CA, June 1–14, pp.1619–1624.
[32] Yang, Y. P., Shih, Y. C., and Chen, J. M., 2016, "Real-Time Torque-Distribution Strategy for a Pure Electric Vehicle With Multiple Traction Motors by Particle Swarm Optimisation," IET Electron. Syst. Transp., **6**(2), pp. 76–87.
[33] Shuai, Z., Zhang, H., Wang, J., Li, J., and Ouyang, M., 2014, "Combined AFS and Control of Four-Wheel-Independent-Drive Electric Vehicles Over CAN Network With Time-Varying Delays," IEEE Trans. Veh. Technol., **63**(2), pp. 591–602.
[34] Prestl, W., Sauer, T., Steinle, J., and Tschernoster, O., 2000, "The BMW Active Cruise Control ACC," SAE Paper No. 2000-01-0344.
[35] Larminie, J., and Lowry, J., 2012, *Electric Vehicle Technology Explained*, Wiley, Hoboken, NJ.
[36] Lu, D., and Ouyang, M., 2014, "Torque-Based Optimal Acceleration Control for Electric Vehicle," Chin. J. Mech. Eng., **27**(2), pp. 319–330.
[37] Nandi, A. K., Chakraborty, D., and Vaz, W., 2015, "Design of a Comfortable Optimal Driving Strategy for Electric Vehicles Using Multi-Objective Optimization," J. Power Sources, **283**, pp. 1–18.
[38] Morimoto, S., Tong, Y., Takeda, Y., and Hirasa, T., 1994, "Loss Minimization Control of Permanent Magnet Synchronous Motor Drives," IEEE Trans. Ind. Electron., **41**(5), pp. 511–517.
[39] Dubhashi, A., and Pelly, B. R., 1989, "A Comparison of IGBTs and Power MOSFETs for Variable Frequency Motor Drives," Fourth Annual IEEE Applied Power Electronics Conference and Exposition, Baltimore, MD, Mar. 13-17, pp. 67–74.
[40] Feng, G., Lai, C., Mukherjee, K., and Kar, N. C., 2016, "Current Injection-Based Online Parameter and VSI Nonlinearity Estimation for PMSM Drives Using Current and Voltage DC Components," IEEE Trans. Transp. Electrification, **2**(2), pp. 119–128.
[41] Lai, J. S., Young, R. W., and McKeever, J. W., 1994, "Efficiency Consideration of DC Link Soft-Switching Inverters for Motor Drive Applications," Power Electronics Specialist Conference (PESC'94), Vol. 2, Taipei, Taiwan, June 20-25, pp. 1003–1010.
[42] Benini, L., Castelli, G., Macii, A., Macii, E., Poncino, M., and Scarsi, R., 2001, "Discrete-Time Battery Models for System-Level Low-Power Design," IEEE Trans. Very Large Scale Integr. (VLSI) Syst., **9**(5), pp. 630–640.
[43] Song, Z., Hofmann, H., Li, J., Han, X., Zhang, X., and Ouyang, M., 2015, "A Comparison Study of Different Semi-Active Hybrid Energy Storage System Topologies for Electric Vehicles," J. Power Sources, **274**, pp. 400–411.
[44] Rambaldi, L., Bocci, E., and Orecchini, F., 2011, "Preliminary Experimental Evaluation of a Four Wheel Motors, Batteries Plus Ultracapacitors and Series Hybrid Powertrain," Appl. Energy, **88**(2), pp. 442–448.
[45] Feng, S., Sun, H., Zhang, Y., Zheng, J., Liu, H. X., and Li, L., 2019, "Tube-Based Discrete Controller Design for Vehicle Platoons Subject to Disturbances and Saturation Constraints," IEEE Trans. Control Syst. Technol. (epub).